

Research

Enhanced Lateral Current Transport Via the Front N^+ Diffused Layer of N -type High-efficiency Back-junction Back-contact Silicon Solar Cells

Filip Granek^{1*,†}, Martin Hermle¹, Dominik M. Huljić², Oliver Schultz-Wittmann^{1‡} and Stefan W. Glunz¹

¹Fraunhofer Institute for Solar Energy Systems (ISE), Heidenhofstr. 2, D-79110 Freiburg, Germany

²Q-Cells AG, Guardianstr. 16, D-06766 Bitterfeld-Wolfen, Germany

N -type back-contact back-junction solar cells were processed with the use of industrially relevant structuring technologies such as screen-printing and laser processing. Application of the low-cost structuring technologies in the processing of the high-efficiency back-contact back-junction silicon solar cells results in a drastic increase of the pitch on the rear cell side. The pitch in the range of millimetres leads to a significant increase of the lateral base resistance. The application of a phosphorus doped front surface field (FSF) significantly reduces the lateral base resistance losses. This additional function of the phosphorus doped FSF in reducing the lateral resistance losses was investigated experimentally and by two-dimensional device simulations. Enhanced lateral majority carrier's current transport in the front n^+ diffused layer is a function of the pitch and the base resistivity. Experimental data show that the application of a FSF reduces the total series resistance of the measured cells with 3.5 mm pitch by $0.1 \Omega \text{ cm}^2$ for the $1 \Omega \text{ cm}$ base resistivity and $1.3 \Omega \text{ cm}^2$ for the $8 \Omega \text{ cm}$ base resistivity. Two-dimensional simulations of the electron current transport show that the electron current density in the front n^+ diffused layer is around two orders of magnitude higher than in the base of the solar cell. The best efficiency of 21.3% was obtained for the solar cell with a $1 \Omega \text{ cm}$ specific base resistivity and a front surface field with sheet resistance of $148 \Omega/\text{sq}$. Copyright © 2008 John Wiley & Sons, Ltd.

KEY WORDS: back-junction; back-contact; high-efficiency; front surface field; Si solar cells

Received 28 April 2008; Revised 27 August 2008

INTRODUCTION

The back-contacted and back-side collecting silicon solar cell design represents a very attractive cell struc-

ture. Sunpower Corporation demonstrated recently manufacturing of this cell type with efficiencies exceeding 22% in its production lines.¹ Low-cost approaches to the high-efficiency back-contact and back-junction (BC BJ) cell structure are being intensively investigated also by other groups, e.g. the RISE cell concept developed at ISFH,² the Quebec cell concept developed by Q-Cells AG in cooperation

* Correspondence to: Filip Granek, Fraunhofer Institute for Solar Energy Systems (ISE), Heidenhofstr. 2, D-79110 Freiburg, Germany.

[†]E-mail: filip.granek@ise.fraunhofer.de

[‡]Now with Solalex Inc., California, USA.

with groups of Fraunhofer ISE and ISFH³ and the IBBC cell concept developed at UNSW.⁴ One of the main advantages of the back-contact and back-junction cell structure is the fact that this cell type has no metal contacts on the front cell side, thus the optical shading losses are avoided. The front side of the cell can be optimised focusing on the optical performance and low recombination, while the rear metallisation can be at the same time optimised focusing on the electrical performance (i.e. minimisation of resistance losses and optimisation of the collection efficiency). This leads to a very high efficiency potential.

High volume manufacturing of the back-contact and back-junction solar cell structure in the industrial environment requires applications of adequate processing technologies. The use of the photolithography technique is not cost-effective. Replacement of the very accurate photolithography with industrially applicable masking steps such as ink-jetting and screen-printing of resist masks or laser processing leads to a significant reduction of the resolution and positioning accuracy, which is especially critical if more than one masking step is used. The pitch on the rear cell side processed with the above mentioned low-cost masking technology increase significantly as schematically shown in Figure 1. Point-contact solar cells processed by the group of Swanson at Stanford University in the 1980s for the concentrator applications with the use of photolithography had a pitch of 45 μm .⁵ Solar cells processed by our group without the photolithography have the pitch distance of around 2 mm. Thus, when applying low-cost patterning techniques, the pitch on the rear side increases by a factor of more than 40. This means that for the majority

carriers (electrons here) the main current transport is transformed from vertical to lateral direction.

Depending on the base resistivity and pitch up to 90% of the series resistance can be contributed to the lateral majority carrier transport. Thus, the lateral current transport is the main resistance loss mechanism reducing the cell efficiency. The cells processed by our group have a phosphorus diffused front surface field (FSF) which is well-known to improve the front side passivation.⁶ In the case of cells with large pitch, the FSF not only improves the front side passivation but also reduces the lateral resistance for the majority carriers and reduces the series resistance of the solar cell. This additional effect of the front surface field is investigated in the present paper. We present a detailed experimental and simulation analysis of the enhanced lateral current transport in the front n^+ diffused layer of the cells processed with low-cost structuring technologies. We show that FSF is beneficial to reduce the series resistance losses in back-junction cells. Our experimental results show that depending on the cell geometry and the base doping the application of FSF reduces the series resistance of the complete cell by 0.1–1.3 Ωcm^2 , which corresponds to a fill factor loss of 1–12% absolute.

FABRICATION OF THE HIGH-EFFICIENCY BC BJ CELLS

A schematic cross-section of the BC BJ n -type Si solar cell structure analysed in our paper is shown in Figure 2. The cells were fabricated from n -type float-zone (FZ) silicon wafers. Final solar cell thickness was about 160 μm . Specific base resistivities of 1 and 8 Ωcm were chosen. In n -type Si wafers with specific resistivities higher than 1 Ωcm , the bulk lifetime of the base material is high enough to enable good minority carrier collection at the rear junction. On the other hand the base resistivity should not be higher than 10 Ωcm due to strongly increased series resistance in the base material, which would lead to significant efficiency losses. The front side is textured with random pyramids and passivated with a lightly doped ($N_{\text{peak}} = 5 \times 10^{18}\text{cm}^{-3}$) and deep diffused (1.4 μm) phosphorus front surface field (FSF) diffusion. The sheet resistance of the FSF (ρ_{FSF}) is 148 Ω/sq . The diffusion profile of FSF was optimised to achieve an optimum front side passivation quality. Our investigations of the surface passivation quality of different FSF diffusion profiles were presented in

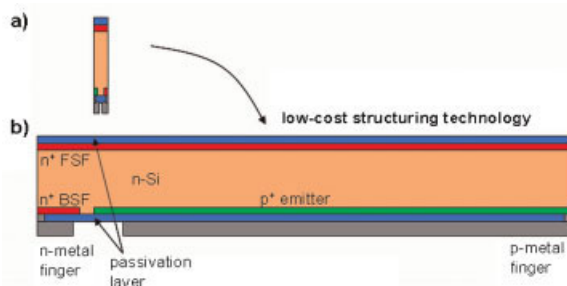


Figure 1. Schematic comparison of a point-contact Si solar cell processed with the use of photolithography with a pitch distance of 45 μm (a) and the solar cell with the use of low cost structuring technology with a pitch distance of 2000 μm (b). Drawings are to scale laterally. Symmetry elements of the cell structures are shown

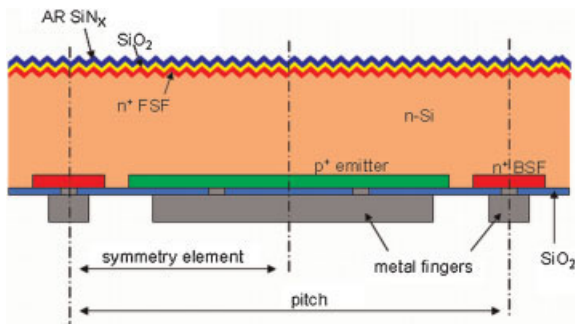


Figure 2. Schematic cross-section of the *n*-type high-efficiency back-contact back-junction silicon solar cell processed at Fraunhofer ISE (sketch is not to scale). Pitch and the symmetry element used for two dimensional device simulations are shown

Reference. 7 The front surface passivation is further improved by the thin thermally grown silicon dioxide layer. Finally a silicon nitride (SiN_x) antireflection layer is deposited on top of the oxide layer by means of plasma enhanced chemical vapour deposition (PECVD). For the masking steps on the rear side such as definition of (i) emitter and (ii) back-surface-field diffusion areas, (iii) local openings in the dielectric layer for the metal-semiconductor contacts and (iv) formation of the interdigitated metal fingers grid, only low-cost screen-printing and laser processes were applied. No photolithography masking steps were introduced to the processing sequence of the investigated cell structure. Due to the fact that more than one masking step was required and because of the lower resolution and positioning accuracy of the applied structuring technology, the resulting pitch of the processed cells was in the range of 1.3–3.5 mm. A simplified rear structure forming an interdigitated *p-n* grid was applied. Both emitter p^+ and back surface field n^+ diffusions are separated by an undiffused gap. The rear cell surface is passivated with silicon dioxide. Metal fingers are contacted to the diffused regions through local openings. Metallisation was performed using a laboratory approach consisting of two steps. First a thin (less than $1\ \mu\text{m}$) seed metal layer was evaporated and structured to form an interdigitated grid geometry. Next, a silver plating process was applied to increase the metal finger height and conductivity. The cells were annealed in forming gas atmosphere. Prior to measurements, the cells were removed from the host wafer by the means of laser cutting with an edge distance of $500\ \mu\text{m}$ from active cell area. This might be too small to avoid all edge recombination losses.⁸

LATERAL CURRENT TRANSPORT OF MAJORITY CARRIERS IN THE FRONT n^+ DIFFUSED LAYER

The emitter coverage on the rear side should be as high as possible to reduce the required diffusion path for the light generated minority carriers to reach the *p-n* junction (see Figure 3). Increased emitter coverage on the rear cell side is linked to a reduced base coverage. As already mentioned before, the pitch of the analysed cell structure was chosen in the range of 1.3–3.5 mm. The emitter coverage on the rear side is of 54–83%, respectively. For the high emitter fraction, the majority carriers (electrons in the case of the *n*-type base material) current need to flow laterally distances in the range of millimetres before reaching the base contacts, which influences the fill factor of the cell. On the other hand, due to lower base coverage on the rear cell side, the minority carriers (holes), which were photo-generated over the base contact regions, have much shorter lateral distances to diffuse resulting in a higher short-circuit current.

Lateral transport of the majority carriers is causing significant series resistance losses due to its larger distances. When a highly doped front n^+ layer is present, the lateral transport of the electrons can be enhanced. In the case of high base resistivity or large lateral distance, the diffused front n^+ layer contribution to the lateral current transport will be significant. This effect is schematically shown in Figure 3.

The so-called *pumping* effect of floating phosphorus doped *n*-type emitter in the *p*-type back-contact back-

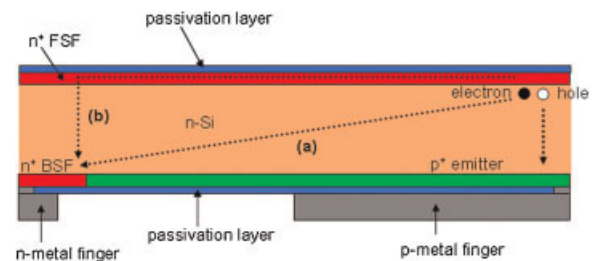


Figure 3. Schematic drawing of the effect of the enhanced lateral current transport of the majority carriers through the front n^+ diffused layer (symmetry element of the cell is shown). For the simplicity reason the front side texture is not shown. The lateral current transport through the front diffused layer (b) can be seen as an additional transport path to the base lateral resistance (a). This way the lateral cell resistance is reduced

junction solar cells has been investigated by Dicker *et al.*⁹ In the case of *p-type* cells with floating emitter, the minority carriers which were photo-generated in large lateral distances from the emitter, are injected to the floating emitter, where they become majority carriers. The lateral flow of these carriers in the floating emitter is enhanced. Next, the carriers are re-injected into the base and diffuse vertically to the *p-n* junction. Thus, the *pumping* effect of the floating emitter reduces the electrical shading losses in the back-contact back-junction cells and therefore should not be confused with the effect of the enhanced lateral current transport in the front diffused n^+ layer, which reduces the lateral resistance losses.

The impact of the pitch on the lateral series resistance in the base of the solar cell can be expressed by the Equation 1, analogous to the series resistance model for the concentrator BC BJ cells from Reference.¹⁰ The impact of the current transport in the front diffused n^+ layer can be described by a parallel resistance to the base lateral resistance

$$\frac{1}{R_{\text{Base},L}} = \frac{1}{\frac{1}{12} \frac{\rho_{\text{Base}}}{d_{\text{wafer}}} (a_{n-n})^2} + \frac{1}{\frac{1}{12} \rho_{\text{FSF}} (a_{n-n})^2} \quad (1)$$

Where a_{n-n} is the distance between the n^+ - and n^+ -doping, ρ_{Base} is the specific resistance of base, d_{wafer} is the wafer thickness and ρ_{FSF} is the sheet resistance of the front n^+ diffused layer.

Due to the parabolic dependence on pitch, an increase of the pitch from 45 μm , as in the cells processed by Sinton *et al.*⁵ with the use of photolithography, to 2000 μm , as in the cells processed in our group with low-cost masking technology, will result in the increase in the lateral series resistance by a factor of 2000. The application of the front diffused n^+

layer (FSF) will reduce the lateral base resistance, especially for cells with a higher specific base resistivity.





A simple analytical series resistance model of the BC-BJ solar cells was developed based on the resistance model of Mohr.¹⁰ Next to the base lateral resistance, the model takes into account also the vertical base resistance, the contact resistance and the metallisation resistance losses. The impact of the lateral current transport in the front n^+ layer was taken into account as shown in Equation 1. The comparison of the analytical series resistance modelling with the experimental data is presented in the next sections.

EXPERIMENTAL

Back-contact back-junction *n-type* silicon solar cells with pitches of 1.3, 1.8, 2.2 and 3.5 mm were fabricated (see Table I). The pitch and the base and emitter width had to be selected, so that the resolution and positioning accuracy of the cell geometry can be done using low-cost masking steps such as screen-printing and laser ablation. The width of the emitter area (p^+) was varied in the range of 700–2900 μm in order to investigate the lateral current transport in base and in front n^+ layer. The width of the base doping on the rear side (undiffused gap and BSF areas) was fixed at 600 μm for all investigated pitches. The resulting emitter fraction on the rear cell side was thus varying in the range of 54% for pitch of 1.3 mm to 83% for pitch of 3.5 mm.

The size of the active cell area is $2 \times 2 \text{ cm}^2$. The busbars ($2 \times 0.15 \text{ cm}^2$) were not included in the cells measurements in order to eliminate series resistance and recombination losses due to busbars, and thus to be

Table I. Photographs and the geometry parameters of the rear side of the back-contacted solar cells with different pitches

p-bus side				
n-bus side				
Emitter [μm]	700	1200	1600	2900
Base [μm]	600	600	600	600
Pitch [μm]	1300	1800	2200	3500
Emitter fraction [%]	54	67	73	83

able to focus on the pitch related two-dimensional effects.

The experimental study was accompanied by two-dimensional device simulations using a numerical device simulation program Sentaurus Device^{TM, 11}. The symmetry element of the device used in the simulations is shown in Figure 2. Busbars and edge effects were not regarded in the simulations.

RESULTS

Best solar cell results for different pitch distances and base resistivities are summarised in Table II. Results in the Table II are the designated cell area (2 cm × 2 cm) measurements, i.e. the busbars were not illuminated during the measurements. The edge area was also not illuminated during the cell measurements. The number of cells in each group was between 1 and 4.

The best efficiency of 21.3% was obtained for a base resistivity of 1 Ω cm and a pitch of 1.8 mm. This result was confirmed by a measurement in the ISE CalLab. Optimal pitch was found to be 1.8–2.2 mm. This optimum represents the best trade-off between emitter coverage on the rear side and series resistance losses due to the increased lateral distances.

As shown in Figure 4 the short-circuit current increases with increasing emitter coverage and reduced base areas of lower minority carrier collection probability. The base width is 600 μm, so in the extreme case, when the photo-generation occurs in the middle of the base area, the minority carriers need to diffuse 300 μm laterally before reaching the *p-n* junction. This leads to recombination in the base material, or at the rear cell side. For the base resistivity of 8 Ω cm and a pitch of 3.5 mm, a maximum J_{SC} of 40.1 mA cm⁻² was obtained. Such a high J_{SC} value

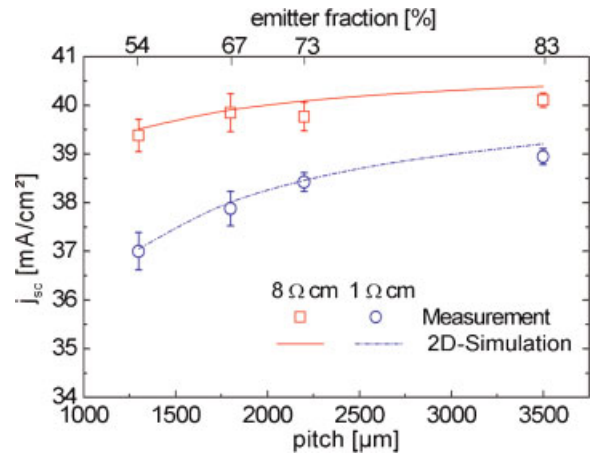


Figure 4. Short-circuit current of the cells with the FSF ($\rho_{FSF} = 148 \Omega/\text{sq}$) and with two specific base resistivities of 1 and 8 Ω cm in the investigated pitch range. The percentage of the emitter fraction on the rear side is shown on the top scale. Points represent experimental results and the lines are the two-dimensional simulation results

indicates very good optical and recombination characteristics of the cell. 2-D device simulations also shown in Figure 4 are in a very good agreement with the experimental results, proving the accuracy of our model. The short-circuit current density of the 1 Ω cm cells was more than 1 mA cm⁻² lower than J_{SC} of the cells with 8 Ω cm specific base resistivity. This effect cannot be explained with the differences in the bulk lifetime of 1 and 8 Ω cm wafers. The effective bulk lifetime of the *n-type* FZ wafers used for the solar cell processing measured with the quasi-steady-state photoconductance (QSSPC) method¹² is 1.2 ms for 1 Ω cm and 10.1 ms for 8 Ω cm.¹³ These lifetime values result in diffusion length of the minority carriers of

Table II. IV-parameters for the best solar cells with a FSF and with the different pitches. Results of the cells with base resistivity of 1 Ω cm (left column) and 8 Ω cm (right column) are presented. Results in the table are the designated cell area (2 × 2 cm²) measurements

Pitch [μm]	$\rho_{base} = 1 \Omega \text{ cm}$					$\rho_{base} = 8 \Omega \text{ cm}$			
	Emitter fraction [%]	J_{SC} [mA cm ⁻²]	V_{OC} [mV]	FF [-]	η [%]	J_{SC} [mA cm ⁻²]	V_{OC} [mV]	FF [-]	η [%]
1300	54	37.0	663	0.812	19.9	39.4	653	0.792	20.2
1800	67	38.8	665	0.825	21.3	39.9	659	0.786	20.7
2200	73	38.4	663	0.816	20.8	39.8	655	0.778	20.3
3500	83	38.9	662	0.801	20.7	40.1	653	0.757	19.8

1.2 mm for $1\ \Omega\text{cm}$ and 3.5 mm for $8\ \Omega\text{cm}$. These diffusion lengths are significantly higher than four times wafer thickness, and are high enough to enable nearly perfect minority carrier collection by the rear junction. In the 2D simulations the same Shockley-Read-Hall bulk lifetime of 1 ms was assumed for both 1 and $8\ \Omega\text{cm}$ base materials. However, even with the same bulk lifetime for 1 and $8\ \Omega\text{cm}$ solar cells, the simulations show a difference in J_{SC} . The reason of the J_{SC} differences between 1 and $8\ \Omega\text{cm}$ wafers is the increased front surface recombination in the case of the $1\ \Omega\text{cm}$ material in comparison to $8\ \Omega\text{cm}$. A significant difference in the internal quantum efficiency (IQE) at short wavelengths between 1 and $8\ \Omega\text{cm}$ solar cells was measured. IQE of the $1\ \Omega\text{cm}$ solar cells with pitch of $2200\ \mu\text{m}$ equals 94% for wavelength of 400 nm. IQE of the $8\ \Omega\text{cm}$ solar cells with pitch of $2200\ \mu\text{m}$ equals 97% for the same wavelength. The difference between the J_{SC} of cells with both base resistivities determined by the integration of the solar spectrum with the both measured IQEs equals $1.8\ \text{mA cm}^{-2}$. This difference is in a good agreement with the measured values presented in Figure 4. The effect of the increased front surface recombination in the case of the $1\ \Omega\text{cm}$ material in comparison to $8\ \Omega\text{cm}$ has been comprehensively investigated by Hermle *et al.*¹⁴

In opposition to J_{SC} , the FF decreases as the pitch increases due to increased lateral resistance in base, as shown in Figure 5. In order to investigate the pitch

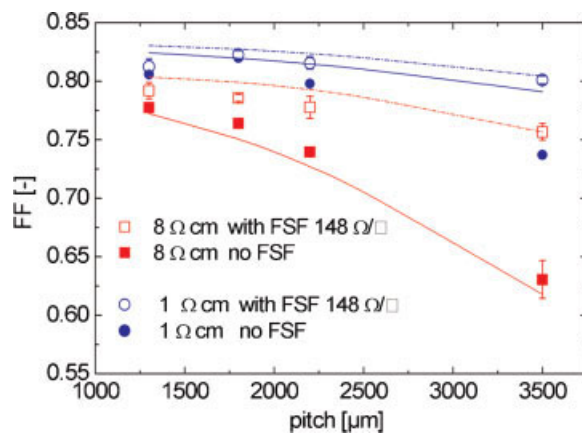


Figure 5. Two-dimensional numerical simulations and measured values of the fill factor of the BC-BJ Si solar cells as a function of the pitch distance for two different base resistivities. Results for the cells with ($\rho_{\text{FSF}} = 148\ \Omega/\text{sq}$) and without FSF diffusion are shown. The data points represent a mean value of the experimental results. Lines represent 2-D simulation results

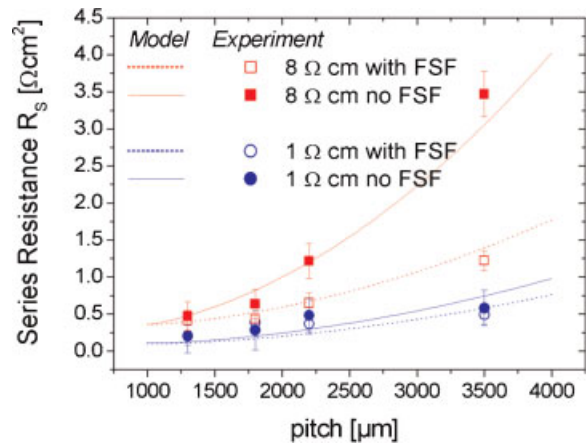


Figure 6. Series resistance of the BC-BJ Si solar cells with different pitches. Results of the cells on 1 and $8\ \Omega\text{cm}$ bulk resistivity and with and without the $148\ \Omega/\text{sq}$ front surface field are presented. The data points represent the mean experimental resistance values of 1–4 cells. The lines represent the simple analytical series resistance model, in which the lateral current transport in the front diffused n^+ layer was taken into account as described by equation 1. In the analytical model the base specific resistivity was adjusted for the conductivity modulation at the maximum power point

related resistance losses, the total series resistance R_s of the processed cells was determined. The series resistance was determined by comparing the Suns- V_{OC} curve¹⁵ with the one-sun IV-curve. For more details on this method to determine the series resistance see for example.¹⁶ The experimentally determined series resistance is presented in Figure 6 together with the analytical series resistance modelling.

Since the series resistance reduces the maximal output power of the solar cell, the analytical model should describe the series resistance at the maximum power point (MPP) conditions. The base resistivity depends strongly on the density of the electrons in the base, and hence can be influenced by the cell operating conditions. Therefore, in order to correctly describe the impact of the base resistance on the total series resistance of the solar cell, the base conductivity modulation at MPP conditions should be taken into account. In the Figure 7 the two-dimensional simulation of the electron density in the base in the voltage range of 0.3–0.7 V is presented. The voltage at maximum power point for 1 and $8\ \Omega\text{cm}$ base resistivities is marked in the graph. The electron density at MPP is higher than the base doping. The base resistivity at MPP is therefore reduced in

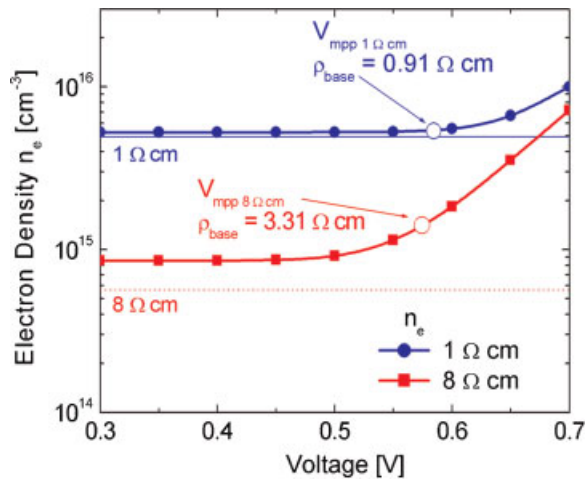


Figure 7. Two-dimensional simulation of the electron density in the base of the BC-BJ solar cells for two specific base resistivities of 1 and 8 Ω cm. The electron density was calculated in the voltage range of 0.3–0.7 V, in a distance of 100 μ m from the top cell surface. The base conductivity modulation at the maximum power point is shown. Thin lines represent the base doping

comparison to the base resistivity of non-illuminated samples. At MPP conditions the base resistivity equals to 0.91 Ω cm for the specific base resistivity of 1 Ω cm, and 3.31 Ω cm for base resistivity of 8 Ω cm. The effect of conductivity modulation at maximum power point was taken into account in the analytical modelling. As shown in Figure 6 a very good agreement between the experimental data and the analytical modelling of series resistance adjusted for the conductivity modulation at MPP conditions proves validity of the analytical model.

For the 1 Ω cm cells with FSF diffusion the series resistance R_S increases starting from 0.2 Ω cm² for the lowest pitch of 1.3 mm to 0.5 Ω cm² for pitch of 3.5 mm. The FF of these cells drops at the same time by about 1% absolute causing around 0.3% absolute efficiency loss. For the case of the 1 Ω cm cells without FSF the increase of R_S is higher. For the largest pitch R_S reaches 0.6 Ω cm².

The solar cells with a base resistivity of 8 Ω cm have a much higher lateral base resistance than the 1 Ω cm cells. This results in a lower FF even for the smallest pitch of 1.3 mm. Moreover the fill factor drop with the increasing pitch is significantly larger than in the case of 1 Ω cm material. For the pitch distance of 1.3 mm a maximal FF of 79% and 78% for 8 Ω cm cells with and without FSF respectively was measured. When reach-

ing the largest pitch of 3.5 mm, FF dropped to 76% for cells with FSF and to 63% for cells without FSF. An absolute FF drop by 3% for the cells with FSF was caused by the increase of R_S from 0.36 Ω cm² for pitch of 1.3 mm to 0.96 Ω cm² for pitch of 3.5 mm. At the same time the FF of the 8 Ω cm cells without FSF dropped by 15%_{abs}, due to increase of R_S from 0.4 to 2.3 Ω cm². The drop in fill factor of our cells is consistent with the series resistance model of Mette,¹⁷ which predicts a drop of FF from 4.5 to 5.5%_{abs} due to an increase of series resistance by 1 Ω cm².

The measured fill factor and 2D simulation are shown in Figure 5. Again, a very good agreement between the experimental and 2D simulation results can be observed. Results shown in Figure 5 clearly demonstrate that the FSF significantly reduces the series resistance losses and thus improves FF in comparison to cells without FSF. The effect of enhanced current transport in the front n^+ diffuse layer is stronger for larger pitches, where the base lateral resistance dominates the resistance losses of the cell. Moreover, the additional impact of the FSF is, as expected, a function of the base doping. For higher base resistivity (8 Ω cm) and large pitch distance (3.5 mm) the FF of the cells with FSF is up to 10% abs. higher than FF of the cells without the FSF.

In order to prove that the decrease in FF for larger pitch distances is only caused by the increased lateral series resistance and not other detrimental effects on the IV curve, the pseudo fill factor (PFF) was measured using the Suns- V_{OC} measurement technique¹⁵ (see Figure 8). The PFF is free from series resistance. As expected the PFF is independent of the pitch. In the analysed pitch range PFF is higher than 82% for 1 Ω cm and higher than 81% for 8 Ω cm solar cells. Such a high PFF of the finished cells indicates that there are no significant shunting and space charge recombination losses in the analysed solar cells. Constant PFF values in the analysed pitch range prove that the variations in FF observed in Figure 5 are caused only by the increasing of series resistance with increasing emitter width.

The two-dimensional simulations of the majority carriers current transport are shown in Figure 9. Here the extreme case of the largest pitch of 3.5 mm was analysed. Enhanced electron current density in the front n^+ diffuse layer area is shown in detail (right side). The electron current density in the n^+ diffused layer area is around two orders of magnitude higher than in the base. This simulation shows that the lateral electron current transport takes not only place in the

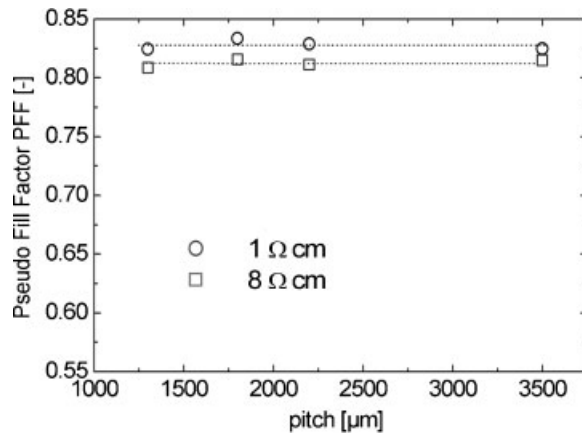


Figure 8. Pseudo Fill Factor (PFF) of the BC-BJ solar cells with different pitches. Experimental results for the solar cells with FSF and base resistivity of FSF and 1 and 8 Ω cm material are shown. No reduction of PFF over a wide pitch range was observed. Lines are guides-to-the-eye

base, but also in the front diffused n^+ layer. The electrons, which were photo-generated at the front cell side in the first few micrometers of the wafer, take the advantage of the high conductivity of the front n^+ layer

until they are above base contacts and then a vertical current transport through the base thickness takes place.

The vertical profiles of the electron current density through the thickness of the solar cell were taken in the vicinity of the base contacts (A-B cut in Figure 9). These profiles for 1 and 8 Ω cm specific base resistivities are shown in Figure 10. A significant difference in the fraction of the current transport in the front diffused region and the base between the two base resistivities can be observed. After integrating the current density profiles, it was found that for the specific base resistivity of 1 Ω cm 27% of the lateral electron current transport takes place in the front n^+ layer. The remaining 73% of the current flows laterally through the base. A simple parallel resistance circuitry, as introduced by the analytical model in Equation 1, can be applied to clarify the current sharing between base and n^+ front region. For the specific base resistivity of 1 Ω cm and the wafer thickness of 160 μ m the wafer sheet resistance equals 42 Ω /sq. The base resistance is in parallel with n^+ sheet resistance of 148 Ω /sq. This implies a current sharing of 29% for the front n^+ region and 71% for the n -type base. Thus, in the case of base resistivity of 1 Ω cm the analytical modelling matches

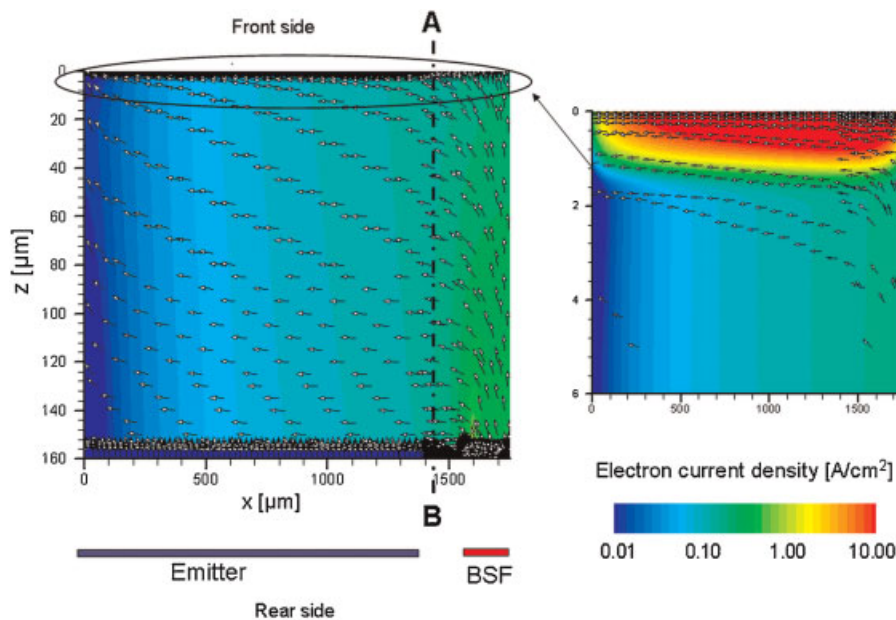


Figure 9. Two-dimensional modelling results of the lateral and vertical electron current transport in the n -type BC-BJ solar cell structure with base resistivity of 8 Ω cm and pitch distance of 3.5 mm. The symmetry element of the solar cell is shown. The arrows show the direction opposite to the electron flow at V_{MPP} of a cell with front surface field ($\rho_{FSF} = 148 \Omega$ /sq). The A-B cut of the electron current density through the cell thickness is marked

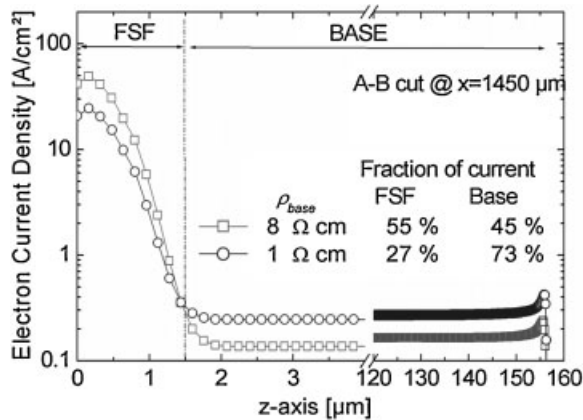


Figure 10. Two-dimensional simulation of the electron current density for cells with 1 and 8 Ω cm specific base resistivity and a FSF ($\rho_{\text{FSF}} = 148 \Omega/\text{sq}$) at the maximum power point conditions. A-B cuts of the electron current density through the wafer thickness for both base resistivities are shown. Front side of the solar cell corresponds to $z = 0$. Areas of the FSF and the base are indicated in the graph. Fractions of the current flow in the front n^+ diffused layer and the base for both specific base resistivities are shown

the two-dimensional modelling presented in Figure 10 very well. The analysis of the 2-D simulation of the cells with base resistivity of 8 Ω cm, shows that the contribution of the front diffused area to the lateral current transport of the majority carriers becomes dominant and increases to 55%, with 45% of the current transport taking place in the base. The application of the same simple parallel resistance circuitry here would result in the current sharing of 77% in the front diffused region and 23% in the base. These results are not in an agreement with 2-D simulations. However, if the same calculation is repeated for the base resistance corrected for conductivity modulation at MPP ($\rho_{\text{base}} = 3.31 \Omega$ cm instead of 8 Ω cm), the base would carry 42% of the current and the front diffused layer would carry 52% of the current. These results match the simulation results very well. This shows the importance of the using the two-dimensional modelling, when describing the solar cell which does not operate in low injection conditions.

CONCLUSION

N-type back-contact back-junction solar cells were processed with the use of industrially relevant

structuring technologies such as screen-printing and laser processing, resulting in the best efficiency of 21.3% on 1 Ω cm specific base resistivity and with a front surface diffusion of 148 Ω/sq . If the low-cost structuring technology is applied in the processing of the BJC cell structure, the pitch on the rear side of the cell drastically increased to values in the range of millimetres. This significantly increases the lateral base resistance. Our investigations show that the introduction of the phosphorus doped front surface field significantly reduces the lateral base resistance losses. The majority carriers which were photo-generated in large lateral distances from the base contacts and which were generated on the front cells side, take the advantage of the high conductivity of the front diffused n^+ layer in order to reduce its resistance losses. This additional function of the FSF in reducing the lateral resistance losses could be demonstrated by experiments and two-dimensional device simulations. The experimental solar cell results and two-dimensional simulation results are in a very good agreement. As expected the enhanced lateral majority carrier's current transport in the front diffused n^+ layer is a function of the pitch and the base resistivity. The introduction of phosphorus diffused FSF reduces the total series resistance of the measured cells with 3.5 mm pitch of 0.1 Ω cm² for the base resistivity and 1.3 Ω cm² for the 8 Ω cm base resistivity. According to the two-dimensional simulations of the electron current transport, the electron current density in the front diffused n^+ layer is around two orders of magnitude higher than in the base of the solar cell.

Acknowledgements

The authors thank Sonja Seitz, Antonio Leimenstoll, Christian Harmel and Anke Herbolzheimer for the solar cell processing, Elisabeth Schäffer for the measurements and Sven Kluska for the measurement of the series resistance. Fruitful co-operation and many valuable discussions with our partners in Q-Cells AG are gratefully acknowledged. This work is supported by the German Federal Ministry for the Environment, Nature Conservation and Nuclear Safety in frame of the QUEBEC project.

REFERENCES

1. De Ceuster D, Cousins P, Rose D, Vicente D, Tipones P, Mulligan W. Low cost, high volume production of

- >22% efficiency silicon solar cells. *Proceedings of the 22nd European Photovoltaic Solar Energy Conference*, Milan, Italy, 2007; 816–819.
2. Engelhart P, Harder N-P, Grischke R, Merkle A, Meyer R, Brendel R. Laser structuring for back junction silicon solar cells. *Progress in Photovoltaics: Research and Applications* 2006; **15**: 237–243.
 3. Huljic D, Zerres T, Mohr A, Maydell Kv, Petter K, Müller JW, Feist H, Harder N-P, Engelhart P, Brendemühl T, Grischke R, Meyer R, Brendel R, Granek F, Grohe A, Hermle M, Schultz O, Glunz SW. Development of a 21% back-contact monocrystalline silicon solar cell for large-scale production. *Proceedings of the 21st European Photovoltaic Solar Energy Conference*, Dresden, Germany, 2006.
 4. Guo J-H, Tjahjono BS, Cotter JE. 19.2% efficiency n-type laser-grooved silicon solar cells. *Proceedings of the 31st IEEE Photovoltaic Specialists Conference*, Orlando, USA, 2005; 983–986.
 5. Sinton RA, Kwark Y, Gruenbaum P, Swanson RM. Silicon point contact concentrator solar cells. *Proceedings of the 18th IEEE Photovoltaic Specialists Conference*, Las Vegas, Nevada, USA, 1985; 61–65.
 6. King RR, Sinton RA, Swanson RM. Front and back surface fields for point-contact solar cells. *Proceedings of the 20th IEEE Photovoltaic Specialists Conference*, Las Vegas, Nevada, USA, 1988; 538–544.
 7. Granek F, Reichel C, Hermle M, Huljic DM, Schultz O, Glunz SW. Front surface passivation of n-type high-efficiency back-junction silicon solar cells using front surface field. *Proceedings of the 22nd European Photovoltaic Solar Energy Conference*, Milan, Italy, 2007; 1262–1265.
 8. Sinton RA, Verlinden PJ, Swanson RM, Crane RA, Wickham K, Perkins J. Improvements in silicon back-side-contact solar cells for high-value one-sun applications. *Proceedings of the 13th European Photovoltaic Solar Energy Conference*, Nice, France, 1995; 1586–1589.
 9. Dicker J, Schumacher JO, Warta W, Glunz SW. Analysis of one-sun monocrystalline rear-contacted silicon solar cells with efficiencies of 22.1%. *Journal of Applied Physics* 2002; **91**: 4335–4343.
 10. Mohr A. Silicon concentrator cells in a two-stage photovoltaic system with a concentration factor of 300x. In *Fakultät für Angewandte Wissenschaften*. Universität Freiburg: Freiburg, 2005; 156.
 11. Synopsys Zurich, Switzerland, TCAD SDEVICE Manual (2007) Release: Z-2007.03, www.synopsys.com
 12. Sinton RA, Cuevas A, Stuckings M. Quasi-steady-state photoconductance, a new method for solar cell material and device characterization. *Proceedings of the 25th IEEE Photovoltaic Specialists Conference*, Washington DC, USA, 1996; 457–460.
 13. Granek F, Hermle M, Fleischhauer B, Grohe A, Schultz O, Glunz SW, Willeke G. Optimisation of laser-fired aluminium emitters for high efficiency n-type Si solar cells. *Proceedings of the 21st European Photovoltaic Solar Energy Conference*, Dresden, Germany, 2006; 777–780.
 14. Hermle M, Granek F, Schultz O, Glunz SW. Analyzing the effects of front-surface fields on back-junction silicon solar cells using the charge-collection probability and the reciprocity theorem. *Journal of Applied Physics* 2008; **103**: 054507/1–7.
 15. Sinton RA, Cuevas A. A quasi-steady-state open-circuit voltage method for solar cell characterization. *Proceedings of the 16th European Photovoltaic Solar Energy Conference*, Glasgow, UK, 2000; 1152–1155.
 16. Pysch D, Mette A, Glunz SW. A review and comparison of different methods to determine the series resistance of solar cells. *Solar Energy Materials & Solar Cells* 2007; **91**: 1698–1706.
 17. Mette A. New concepts for front side metallization of industrial silicon solar cells. In *Fakultät für Angewandte Wissenschaften*. Universität Freiburg: Freiburg, 2007; 231.